Application of centrifugal filter to aerosol size distribution measurement

Application of centrifugal filter to aerosol size distribution measurement

Yutaka Tanaka[a], Hyun-Jin Choi[b], Kosuke Shimadzu[a], Hidenori Higashi[b], Takafumi Seto[b], Mikio Kumita[b], Yoshio Otani[b]

[a] Graduate School of Natural Science and Technology, Kanazawa University, Kakuma-machi, Kanazawa, Ishikawa 920-1192, Japan

[b] Institute of Science and Engineering, Kanazawa University, Kakuma-machi, Kanazawa, Ishikawa 920-1192, Japan

Address correspondence to Mikio Kumita, Institute of Science and Engineering, Kanazawa University, Kakuma-machi, Kanazawa, Ishikawa 920-1192, Japan

E-mail: kumita@se.kanazawa-u.ac.jp

ABSTRACT

In the present work, the centrifugal filter proposed by the authors (Nakajima et al. 2015) was applied to classify aerosol particles followed by the detection of total mass or number concentrations so as to measure the size distribution of aerosol particles. The structure and operating condition of the centrifugal filter were optimized in order to attain sharp separation curves with various cut-off sizes between 0.3 and 10 μm. The aerosol penetrating the centrifugal filter at various rotation speeds was measured with a photometer to determine the total mass concentration. The virtue of this system is that the cut-off size is varied just by scanning the rotation speed of filter and that it can be applied to the measurement of high concentration aerosols without dilution by choosing an appropriate filter medium. As a result, the centrifugal filter was successfully applied to measure the size distribution of solid particles in size ranging from 0.3 to 10 μm.

1. Introduction

We have proposed a new type of air filter "centrifugal filter" in which a cylindrical filter rotates along the axis parallel to the air flow (Nakajima et al. 2015). The collection efficiency of the centrifugal filter is adjustable by changing the rotation speed without changing the pressure drop. In addition to this, the centrifugal force exerts on particles perpendicular to the air flow so that the re-entrained particles would not reenter the filtered air. These advantages of the centrifugal filter make its application as a classifier for high concentration of aerosols. There are several measuring instrument available for sizing particles in the size range of 0.3 to 10 μm, e.g., an optical particle counter (OPC), Anderson air sampler (AAS), and Aerodynamic particle sizer (APS) (Baron 1986; Cheng et al. 1993; Sachweh et al. 1998; Hinds 1999; Dunbar et al. 2005; McMurry 2005; Binnig et al. 2007). The OPC can measure only low concentrations of aerosol commonly less than 1000 cm^{-3} based on the optical size because of significant coincidence error at a high concentration (Hinds 1999; Sachweh et al. 1998; Binnig et al. 2007). The AAS is a multi-stage orifice impactor used to measure the size distribution based on the aerodynamic size but it requires the weighing of collected particles on the individual stages so the measurement cannot be conducted in real time. The APS can measure the particle size between 0.1 to 20 μm according to the aerodynamic size. The measureable concentration of APS is limited to a low level because it is also affected by the coincidence error (Baron 1986; Cheng et al. 1993; Hinds 1999; Binnig et al. 2007). Therefore, an instrument which measures the size distribution of high-concentration aerosol particles in the range of 0.3 to 10 μm based on the aerodynamic size in real time is missing.

Since the collection efficiency of the centrifugal filter is varied by changing the rotation speed of filter to attain various cut-off sizes, it may be combined with a particle detector which does not have size-discrimination capability to form a new type of measurement system. By scanning the rotation speed of the centrifugal filter followed by the detection of total aerosol concentration, and applying an appropriate inversion scheme from the particle penetration to the size distribution, we may construct a real time aerosol measurement system based on the aerodynamic size as SMPS measures the size distribution based on mobility diameter by scanning the voltage.

In the present work, the structure of the centrifugal filter for classifying particles is optimized to attain a sharp cut-off curve and the classification performance of the centrifugal filter is investigated by using monodispersed PSL particles. Then the centrifugal filter combined with a photometer is applied to the measurement of polydispersed particles.

2. Optimization of filter structure for aerosol classification

The structure of the centrifugal filter is shown in Figure 1 (Nakajima et al. 2015). A cylindrical filter or porous media is mounted in a filter holder and the filter holder is connected to the inlet and outlet tubes via rotary joints. The filter holder is rotated by an external motor via a belt or a gear. The collection efficiency of the centrifugal filter is predicted by using the classical filtration theory accounting for inertia, interception, gravitational settling, Brownian diffusion and centrifugal force (Nakajima et al. 2015).

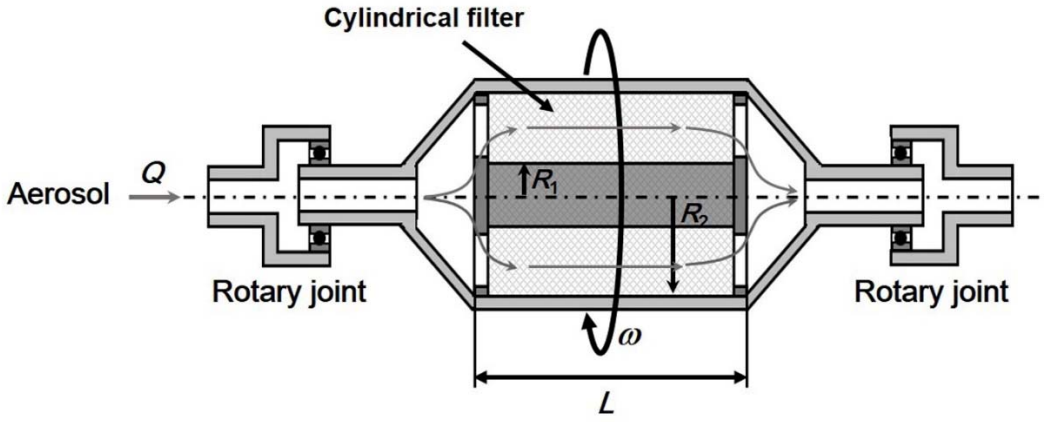

Figure 1. Structure of centrifugal filter.

Table 1. Design parameters of centrifugal filter for aerosol classification.

Volumetric flow rate of aerosol, Q	[L/min]	7
Inner radius of filter, R_1	[mm]	10
Outer radius of filter, R_2	[mm]	40
Filter depth, L	[mm]	40
Maximum rotation speed, ω	[rpm]	3000
Particle size range measured, D_p	[μm]	0.3 – 10

In order to design a classifier with the centrifugal filter the design parameters are assigned as shown in Table 1. The targeted particle size range for the measurement is 0.3 to 10 μm, which is the same size range of OPC. This size range accounts for the size range of ambient particles and is great concern in regards to $PM_{2.5}$. Under the constraints of design parameters, the structure of filter is optimized with respect to filter properties (namely, the fiber diameter and the packing density) as well as the filtration velocity. Figure 2 shows the separation curves of the centrifugal filter at various rotation speeds for filters with the fiber diameters of, respectively, 100, 200 and 300 μm.

As shown in Figure 2, the slopes of the separation curves are the same for filters with different fiber sizes although they are different without the filter rotation. This is because the single fiber collection efficiency due to the centrifugal force is given simply by the ratio of terminal centrifugal settling velocity, v_c, to the filtration velocity, u_0:

$$\eta_c = \frac{v_c}{u_0} \tag{1}$$

$$v_c = v_t\left(\frac{r\omega^2}{g}\right) = \frac{C_c\rho_p D_p^2 r\omega^2}{18\mu} \tag{2}$$

where v_t is the terminal settling velocity by gravity, r the rotation radius which was set equal to the arithmetic mean of inner and outer radii of filter, R_1 and R_2. When the centrifugal force is dominant for particle collection (this is the case for classification of particles by centrifugal force), the centrifugal single fiber efficiency directly gives the filter efficiency using the log penetration equation:

$$E(D_p) = 1 - \exp\left(-\frac{4}{\pi}\frac{\alpha}{1-\alpha}\frac{L}{D_f}\eta\right) \tag{3}$$

where α is the packing density of filter, L the filter thickness, D_f the fiber diameter, and η the single fiber collection efficiency. The single fiber collection efficiency, η, is the sum of single fiber efficiencies due to individual collection mechanism and $\eta = \eta_C$ when the centrifugal force is dominant. Since the power of exponent which determines the slope of the separation curve is proportional to α (for a small value of α), L, ω^2 and inversely proportional to D_f and u_0 from Equations 2 and 3, whatever the values of α, L, D_f and u_0 are, we may have the same value of the power by adjusting the value of ω^2. Therefore, the slope of separation curve is determined solely by D_p^2 and the separation curve shifts along the axis of particle size according to the value of $\alpha L\omega^2/(D_f u_0)$. Consequently, for a given rotation speed, the smaller α and L are, and the larger D_f and u_0 are, we may separate smaller particles. This was a great disappointment and the disadvantage of the centrifugal filter for application to aerosol classification, i.e., we cannot achieve a steeper separation curve by adjusting the filter property and filtration condition.

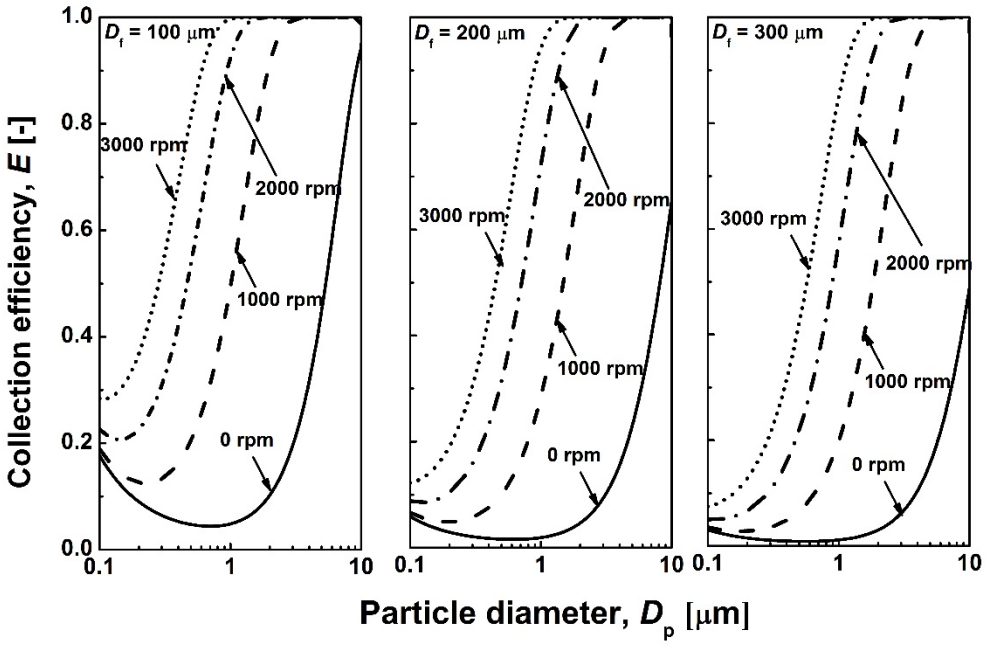

Figure 2. Separation curves of centrifugal filter for various fiber sizes of filter (u_0 = 2.5 cm/s; Q = 7 L/min).

3. Evaluation of separation characteristics of the centrifugal filter

Although we disappointedly found out that we cannot achieve a steeper separation curve, the advantage of adjustable separation curve by changing the rotation speed still remains as an aerosol classifier. As shown in Figure 2, by using either filters with fiber diameter of 100 – 300 μm, we can vary the 50% cutoff diameter from 0.5 to 10 μm by changing the rotation speed from 0 to 3000 rpm, and we may lower the collection efficiency for particles smaller than 0.3 μm by employing a thicker fiber filter. Consequently, we selected polyurethane porous media (Figure 3, the filter properties shown in Table 2) for the centrifugal filter, and the separation characteristics were evaluated with monodispersed PSL particles.

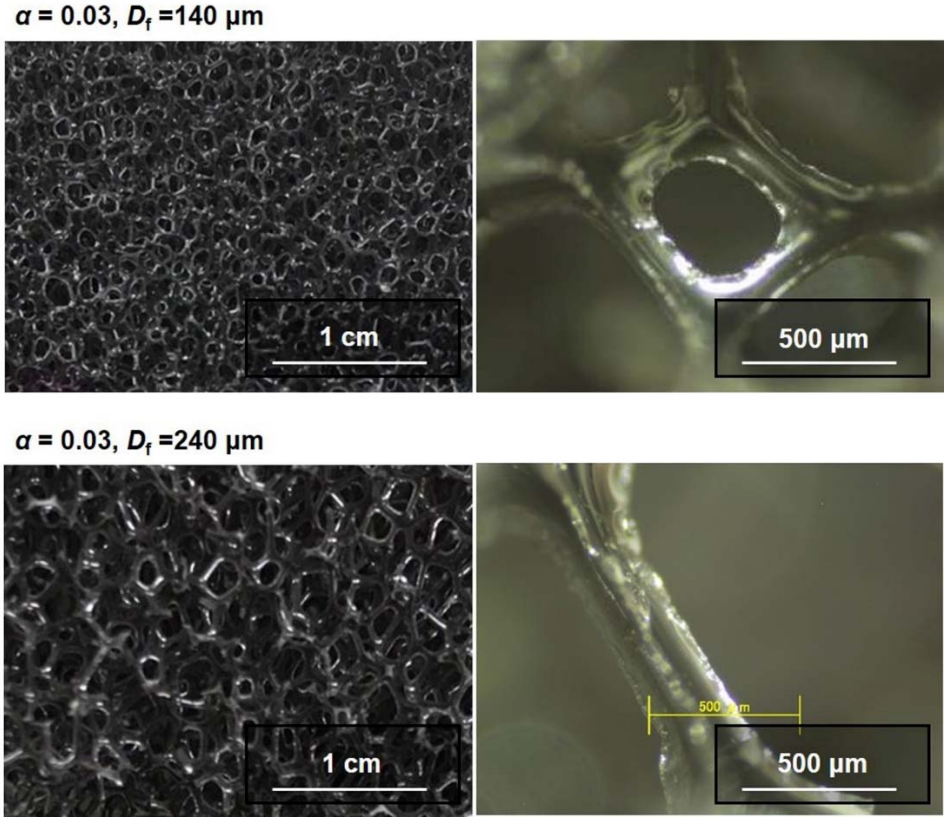

Figure 3. Polyurethane porous media for centrifugal filter.

Table 2. Physical properties of polyurethane foam filters

		Filter 1	Filter 2
Fiber diameter, D_f	[μm]	140	240
Thickness, L	[mm]	40	
Area density, W	[g/m^2]	132	
Packing density, α	[-]	0.03	

Figure 4 shows the experimental setup for the classification performance test of the centrifugal filter by using monodispersed PSL particles. Monodispersed PSL of 0.5, 1.0 and 2.0-μm particles were generated by atomizing the suspension of PSL particles followed by drying with a diffusion dryer. The test particles were neutralized with ^{241}Am neutralizer and mixed with clean air to make the volumetric flow rate equal to 7 L/min. The inlet and outlet concentrations of PSL particles were measured with an optical particle counter (OPS, Model 3330, TSI) by changing the rotation speed of the centrifugal filter.

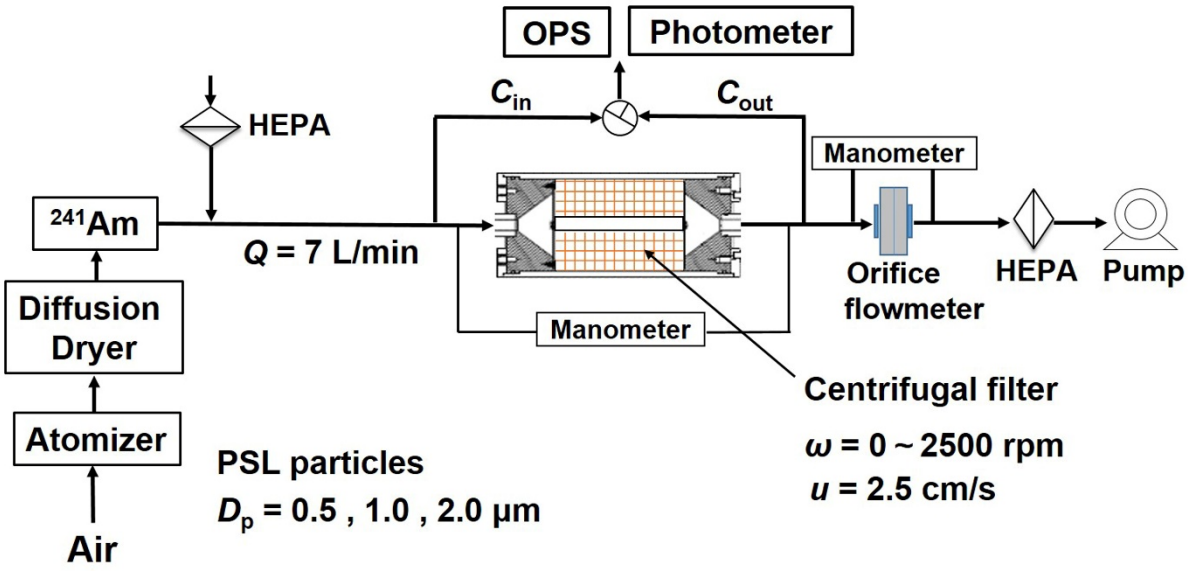

(a)

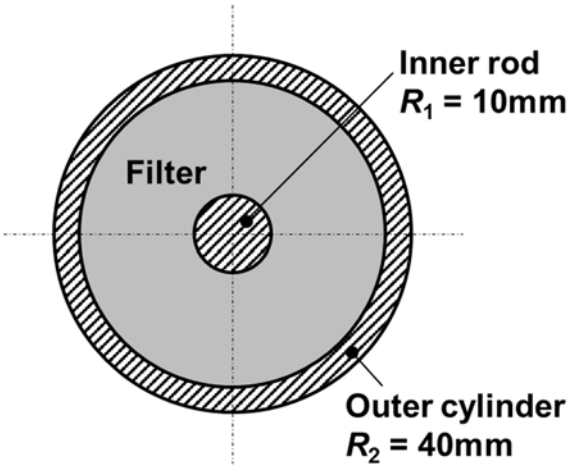

(b)

Figure 4. Experimental setup for: (a) classification performance test of centrifugal filter and (b) cross-sectional image of filter.

Figure 5 shows the change in collection efficiency of monodispersed particles as a function of rotation speed. The left hand side figure of Figure 5 is for filters with fiber diameter of D_{f1} = 140 μm and the right one is for D_{f1} = 240 μm. The lines are those predicted by the classical filtration theory (Nakajima et al. 2015). As seen from these figures, the changes in the collection efficiency of PSL particles with the rotation speed agree well with the predicted lines, indicating that the collection efficiency of the centrifugal filter can be predicted by the filtration theory. Figure 6 compares the separation curves of filters with D_{f1} = 140 μm and D_{f1} = 240 μm by converting the upper abscissa according to $\omega_2 = (D_{f2}/D_{f1})^{1/2}\omega_1$ following the discussion given in the previous section. Figure 6 clearly shows that the separation curves of filters with D_{f1} = 140 μm and D_{f1} = 240 μm agree well each other, confirming that the separation curve cannot be changed by changing the fiber diameter. From Figure 6, we can find the rotation speed

which gives 50% cutoff size of 0.5, 1.0 and 2.0-μm particles for both filters with D_{f1} = 140 μm and D_{f1} = 240 μm, and they are plotted in Figure 7. As seen in this figure, we can alter the 50% cutoff size from 10 μm to 0.3 μm by increasing the rotation speed up to 3000 rpm.

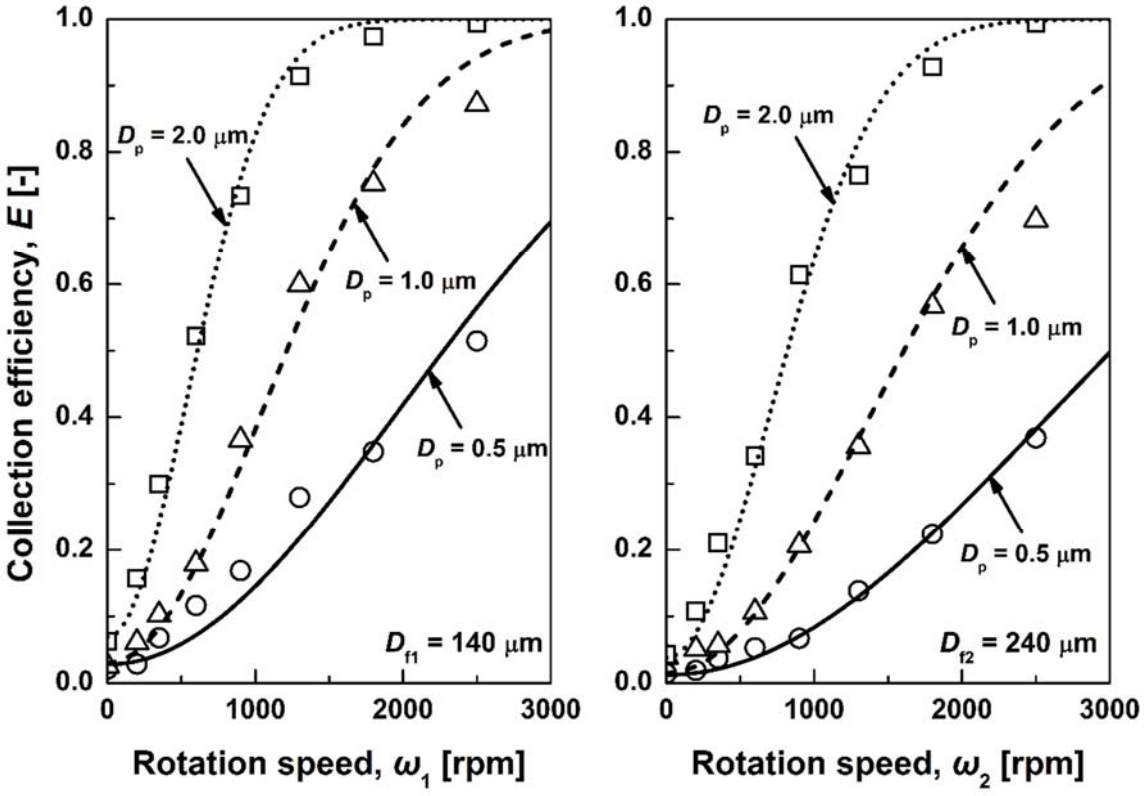

Figure 5. Collection efficiency of monodispersed PSL particles through centrifugal filter as a function of rotation speed at u_0 = 2.5 cm/s.

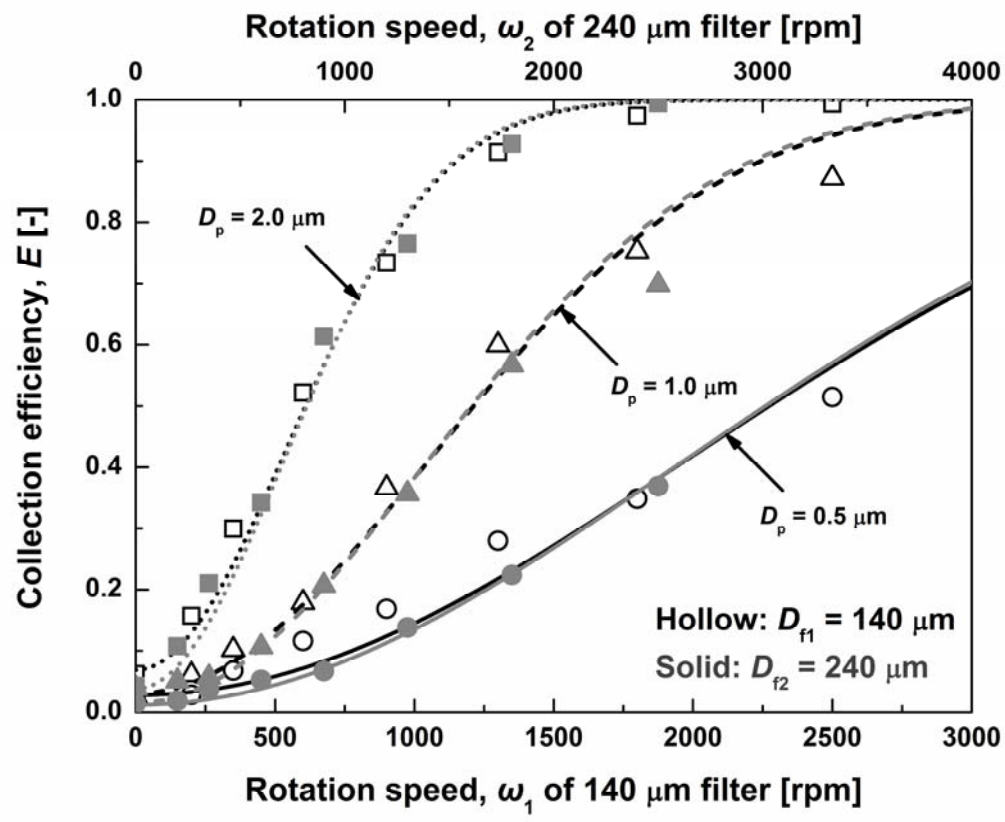

Figure 6. Comparison of collection efficiency of centrifugal filter consisting of 140 μm and 240 μm fibers.

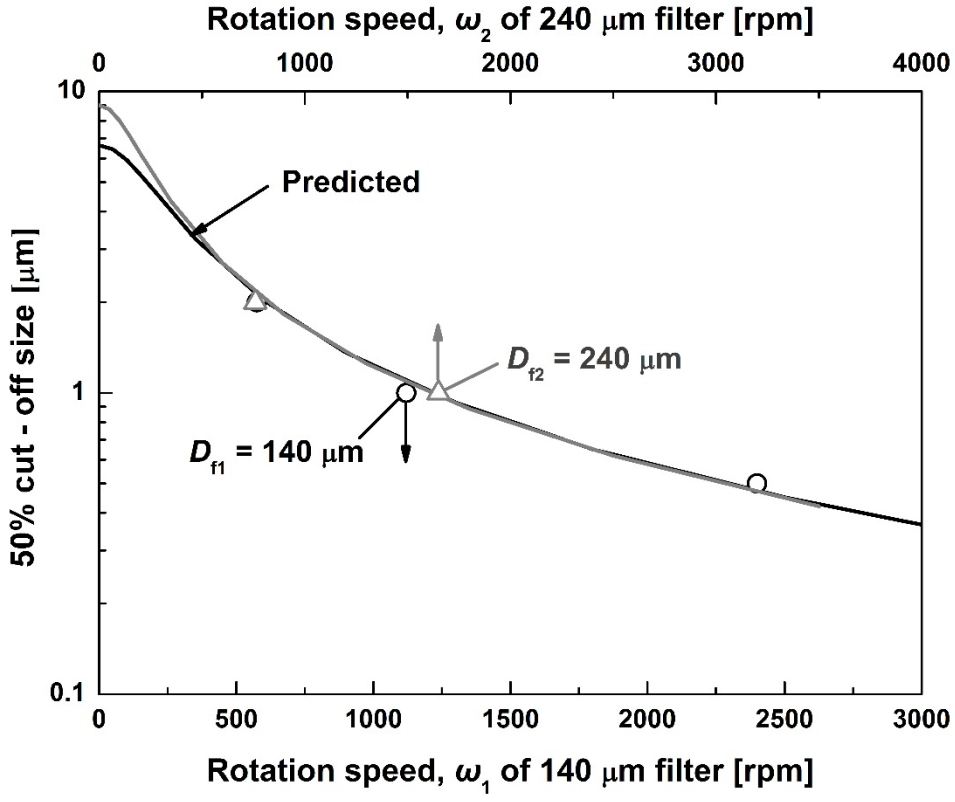

Figure 7. 50% cut-off size of centrifugal filter as a function of rotation speed.

4. Application of the centrifugal filter for polydispersed particles

Since we found that the centrifugal filter functions as predicted by the filtration theory, it was applied to measure the size distribution of polydispersed particles. We used the same experimental setup shown in Figure 4 for the measurement of size distribution of particles, but the atomizer and the diffusion dryer were replaced with a fluidized-bed aerosol generator (Model 3211, Kanomax Inc.). For the detection of particles, a photometer (Dust track, Model 8530, TSI) was employed to determine the total mass concentration in place of the OPS. The OPS was also used to measure the size distribution after the dilution. The test aerosol used was Kanto Loam test dust (JIS Z 8901: Class 11, hereafter referred to as JIS-11) which has the mass median aerodynamic diameter of about 2 μm and the geometric standard deviation of 2.0. The test particles were dispersed by the fluidized-bed aerosol generator and neutralized with the neutralizer. For comparison, the size distribution of JIS-11 was also measured with the AAS (AN-200, Tokyo Dylec Inc.) based on the aerodynamic size.

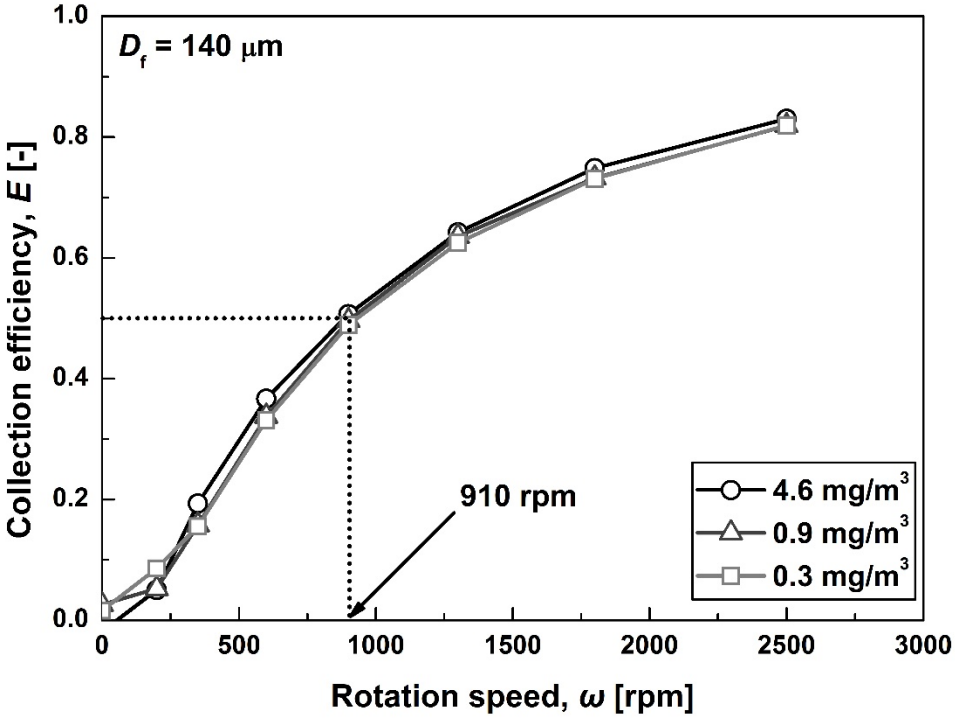

Figure 8. Collection efficiency of JIS-11 particles as a function of rotation speed at various aerosol concentrations.

Figure 8 shows the collection efficiency of JIS-11 particles, which was determined from the ratio of readings of the photometer at the inlet and outlet of the centrifugal filter, as a function of rotation speed at various concentrations of aerosol. We can see from Figure 8 that the aerosol concentration does not affect the collection efficiency of the centrifugal filter and the data are quite reproducible. One may ask questions about how severe the

entrainment of particles from the centrifugal filter is when it is loaded heavily with dust and how the collected particles affect the collection efficiency of the centrifugal filter. In order to answer these questions, we loaded filter with JIS-11 powder (not with the aerosol) by coating the filter with JIS-11 powder. The state of coated filter and the placement of the loaded filter for particle reentrainment measurement are shown in Figure 9. The coated filter was placed upstream of clean filter as shown in Figure 9 to mimic the loading pattern of aerosol particles in a filter (i.e., a filter is loaded more heavily with particles in the frontal portion of the filter according to the log-penetrating equation when loaded with aerosol particles). The reentrainment of particles and the change in collection efficiency with the particle load were measured.

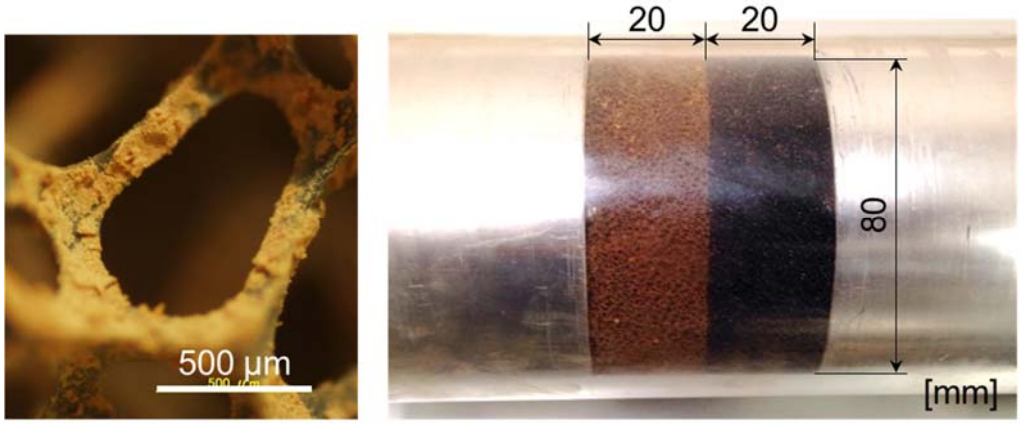

Figure 9. Picture of loaded filter with JIS-11 and the placement of loaded filter upstream of clean filter for particle reentrainment measurement.

Figure 10 shows the change in outlet concentration of the centrifugal filter with the stepwise change in filtration velocity when the filter is loaded at 2.65 kg/m^3 (the loaded mass is the one for the brown layer in Figure 9, determined by weighing the coated filter). When the filter is not rotated, particle reentrainment occurs at the moment of change in filtration velocity. However, when the rotation speed is 500 rpm, the reentrainment is significantly reduced and no entrainment is observed when the rotation speed is 1000 rpm. This is because the reentrained particles are aggregates and large in size so that they are readily captured downstream in the rotating filter. We also conducted an experiment by changing the rotation speed while keeping the filtration velocity (figure is not shown). We did not observe any reentrained particles during change in the rotation speed. Figure 11 shows the change in collection efficiency of particles with the dust load in the centrifugal filter. The fractional collection efficiency remains constant even at the dust load of up to 16 kg/m^3 probably because the single fiber collection efficiency due to centrifugal force is not a function of fiber diameter as given by Equation 1. Therefore, we may conclude that the reentrainment of captured particles does not occur in the centrifugal filter, and that the deposited particles do not change the collection efficiency of the centrifugal filter.

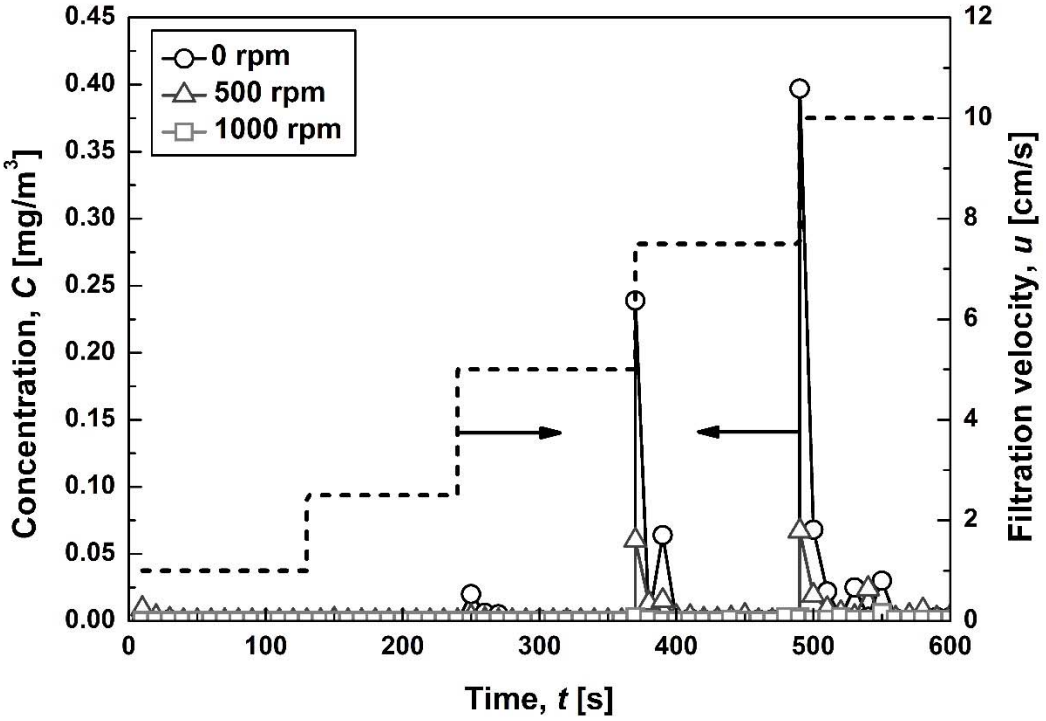

Figure 10. Reentrainment of particles from dust loaded filter with the change in filtration velocity.

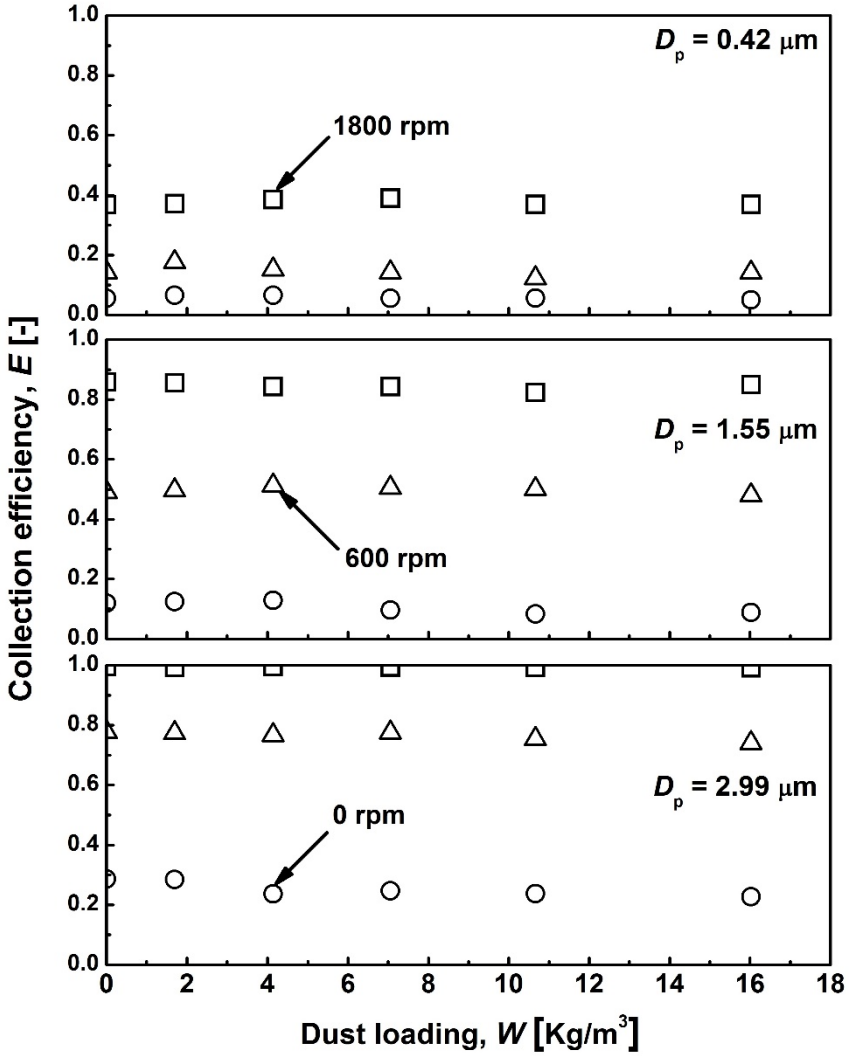

Figure 11. Change in fractional collection efficiency with dust load.

From Figure 8, we can determine the rotation speed which gives 50% collection efficiency to be 910 rpm, and then the 50% cutoff size at 910 rpm is read to be 1.35 μm from Figure 7. The collection efficiency curve of JIS-11 particles is compared with the one predicted by the filtration theory for monodispersed particles of 1.35 μm in Figure 12. The experimental collection efficiency deviates from the predicted curve of monodispersed particles and the deviation should reflect the extent of polydispersity of JIS-11 particles.

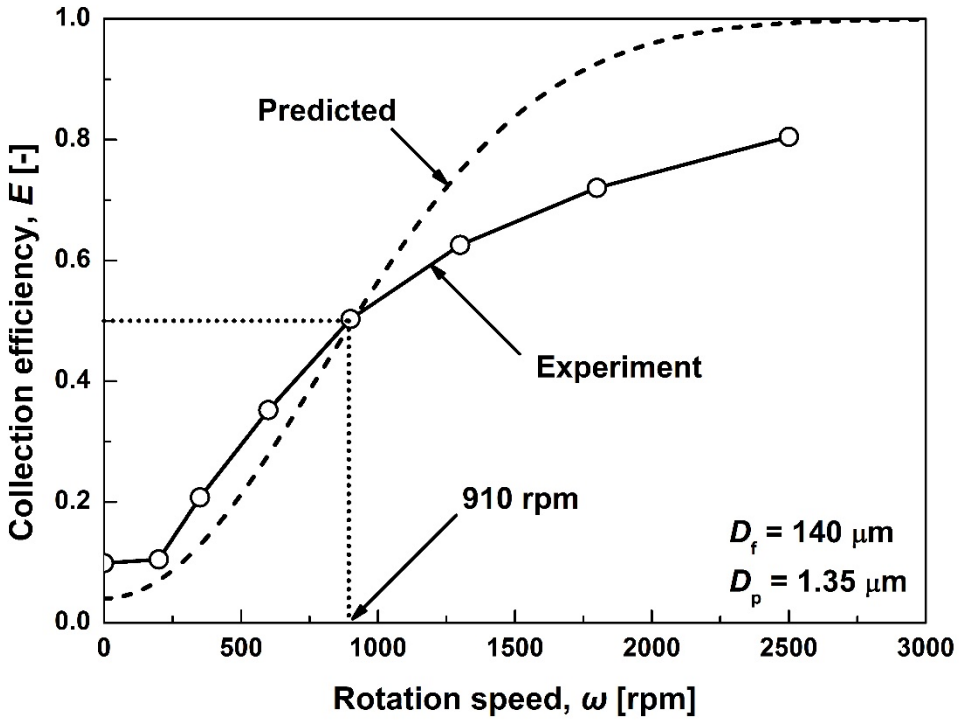

Figure 12. Comparison of collection efficiency of JIS-11 with the one predicted for monodispersed particles of 1.35 μm.

We may retrieve the size distribution of JIS-11 from the efficiency data shown in Figure 12 by employing an appropriate inversion method. For simplicity, we assumed a log normal distribution, and the geometric mean diameter, D_{pg}, and the geometric standard deviation, σ_g, were obtained by using the least square method.

$$f(\ln D_p) = \frac{1}{\sqrt{2\pi}\ln\sigma_g}\exp\left\{-\frac{\left(\ln D_p - \ln D_{pg}\right)^2}{2\ln^2\sigma_g}\right\} \tag{4}$$

The penetration of particles measured by a photometer is given by the following equation assuming that the response of the photometer is proportional to the total projected area of particles:

$$P(D_p) = 1 - E(D_p) = \frac{\int_0^\infty D_p^2 f(\ln D_p, D_{pg}, \sigma_g) P(D_p, \omega) \mathrm{d}\ln D_p}{\int_0^\infty D_p^2 f(\ln D_p, D_{pg}, \sigma_g) \mathrm{d}\ln D_p} \tag{5}$$

Instead of using the particle penetration, here we employed the derivative of particle penetration with respect to the rotation speed in order to extract the influence of the rotation speed:

$$\frac{\partial P}{\partial \omega} = \frac{1}{\int_0^\infty D_p^2 f(\ln D_p, D_{pg}, \sigma_g)\mathrm{d}\ln D_p} \int_0^\infty D_p^2 f(\ln D_p, D_{pg}, \sigma_g) \frac{\partial P(D_p, \omega)}{\partial \omega} \mathrm{d}\ln D_p \tag{6}$$

The tangent of experimental collection efficiency curve was obtained from Figure 8 and the square sum of differences between the experimental one and the one predicted by Equation 6 was minimized to determine the

geometric mean diameter, D_{pg}, and the geometric standard deviation, σ_g:

$$s^2 = \sum_{i=1}^{n} \left\{ \left(\frac{\partial P}{\partial \omega} \right)_i^{\exp} - \left(\frac{\partial P}{\partial \omega} \right)_i^{\text{pred}} \right\}^2 \tag{7}$$

Since the geometric mean diameter, D_{pg}, and the geometric standard deviation, σ_g, are based on particle number, they are converted to D'_{pg} and σ'_g based on mass by using the following Hatch's formula:

$$\begin{aligned} \ln D'_{pg} &= \ln D_{pg} + 3 \ln^2 \sigma_g \\ \sigma'_g &= \sigma_g \end{aligned} \tag{8}$$

Figure 13 compares the size distributions of JIS-11 particles measured by the centrifugal filter, AAS and OPS. We see good agreement between those measured by the centrifugal filter and OPS, and AAS gives the same geometric mean diameter but a little bit smaller slope, i.e., a larger geometric standard deviation. Thus the geometric mean diameter, D_{pg}', measured by the centrifugal filter is equal to 1.8 μm, and the geometric standard deviation, σ_g', is 2.0. Incidentally, OPS measures the optical size and AAS and the centrifugal filter measure the aerodynamic size. However, since JIS-11 particles are brown in color and have a density of 2400 kg/m^3, the optical size and aerodynamic size may coincide with each other, which is one of the merits of using JIS-11 particles as a test aerosol.

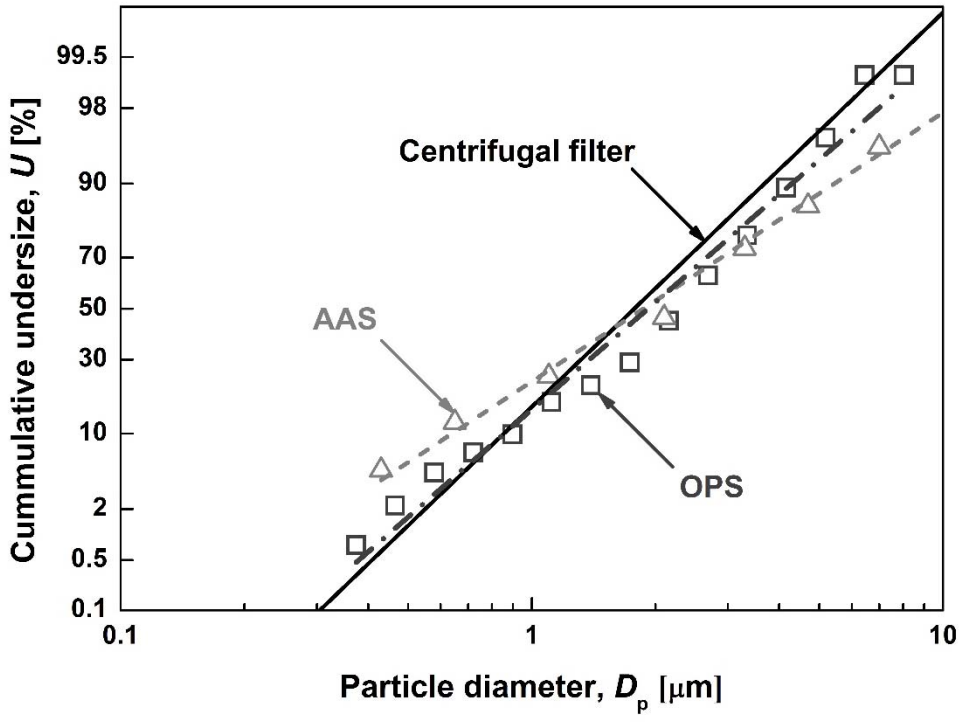

Figure 13. Comparison of size distributions of JIS-11 measured by centrifugal filter, AAS, and OPS.

Figure 14 compares the size distributions measured by the centrifugal filter and OPS for JIS-11 particles after

filtration with a low efficiency filter. We can find good agreement between those measured by the centrifugal filter and OPS and the geometric mean diameter, D_{pg}', and the geometric standard deviation, σ_g', is respectively 1.5 μm and 1.6.

The merit of the centrifugal filter with scanning rotation speed and taking the derivatives of the penetration curve with respect to the rotation speed is such that we can extract the dependence of photometer response on rotation speed for a given aerosol by appropriately choosing the configuration of the centrifugal filter and operating conditions. Furthermore, although an error in particle size measurement usually occurs by the deposition loss of large particles in a measuring instrument, in the present centrifugal filter and photometer system, large particles are readily captured by the rotating filter without the reentrainment thus minimizing the error introduced by the deposition loss of large particles.

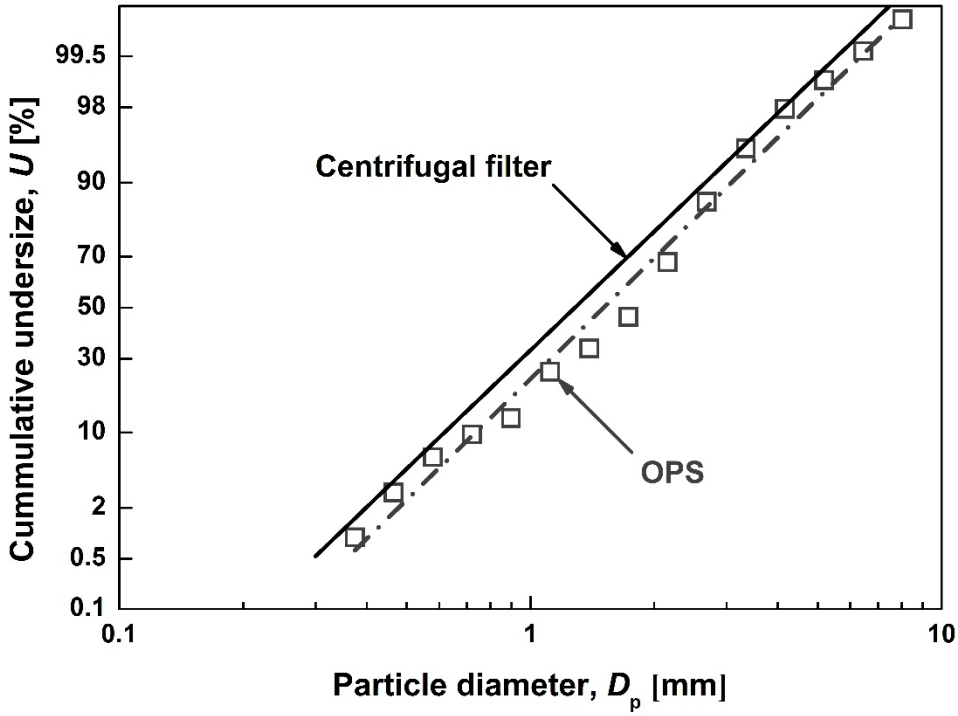

Figure 14. Comparison of size distribution measured by centrifugal filter and OPS for JIS-11 after filtration.

Conclusion

In the present work, the centrifugal filter was applied to classify aerosol particles followed by the detection with a photometer to determine the size distribution of aerosol particles. The structure and operating condition of the centrifugal filter were attempted to be optimized in order to attain a sharp separation curve with various cut-off sizes between 0.5 and 10 μm but we found that the separation curve is invariant with the change in filter property and filtration velocity. The centrifugal filter with a photometer was applied to measure the size distribution of polydispersed particles and we found that the reentrainment of particles from the filter is not significant and that the

collection efficiency does not change with the dust load. As a result, the centrifugal filter can give the size distribution of high concentration aerosols which is in good agreement with the one measured by an optical particle counter.

References

Baron, P. A. (1986). Calibration and use of the aerodynamic particle sizer (APS3300). Aerosol Sci. Technol. 5:55-67.

Binnig, J., Meyer, J., and Kasper, G. (2007). Calibration of an optical particle counter to provide PM2.5 mass for well-defined particle materials. J. Aerosol Sci. 38:325-332.

Cheng, Y. S., Barr, E. B., Marshall, I. A., and Mitchell, J. P. (1993). Calibration and performance of an API aerosizer. J. Aerosol Sci. 24:501-514.

Dunbar, C., Kataya, A., and Tiangbe, T. (2005). Reducing bounce effects in the Andersen cascade impactor. Int. J. Pharmaceut. 301:25-32.

Gard, E., Mayer, J. E., Morrical, B. D., Dienes, T., Fergenson, D. P., Prather, K. A. (1997). Real-time analysis of individual atmospheric aerosol particles: Design and performance of a portable ATOFMS. Anal. Chem. 69:4083-4091.

Hinds, W. C. (1999). Aerosol Technology: Properties, Behavior, and Measurement of Airborne Particles. 2nd ed. Wiley & Sons, New York, p.136.

McMurry, P. H. (2000). A review of atmospheric aerosol measurements. Atmos. Environ. 34:1959-1999.

Nakajima, S., Kumita, M., Matsuhashi, H., Higashi, H., Seto, T., and Otani, Y. (2015). Centrifugal filter for aerosol collection. Aerosol Sci. Technol. 49:959-965.

Sachweh, B., Umhauer, H., Ebert, F., Büttner, H., and Friehmelt, R. (1998). In situ optical particle counter with improved coincidence error correction for number concentrations up to 10^7 particles cm^{-3}. J. Aerosol Sci. 29:1075-1086.